

DOI:10.3969/j.issn.1005-202X.2023.09.008

Medical imaging physics

Cramér-Rao lower bound of dark-field imaging using a grating interferometer

LIU Bo, CHEN Zihan, GU Yao, CHEN Heng, WANG Zhili

Department of Optical Engineering, School of Physics, Hefei University of Technology, Hefei 230009, China

Abstract: In grating-based phase contrast imaging, the phase stepping technique is commonly utilized for data acquisition and signal retrieval from acquired intensity data. However, the algorithm efficiency with respect to the dark-field retrieval has yet to be sufficiently evaluated. Herein the algorithm efficiency of dark-field retrieval based on Cramér-Rao lower bound is evaluated. The theoretical analysis and numerical results demonstrates that fully efficient algorithm is currently available only for 3-step phase stepping technique, and other techniques with more phase steps are all sub-optimal. Quantitatively, the dependence of the algorithm efficiency on the phase step number and the visibility is investigated. It is shown that the phase stepping technique can nearly approach its theoretical optimal efficiency in the case of a low visibility. With a phase step greater than 5, the algorithm efficiency is only 77.4% in the case of a high visibility. The study can provide some reference for signal-to-noise ratio improvement and potential dose optimization in X-ray and neutron grating-based dark-field imaging.

Keywords: dark-field imaging; grating interferometer; Cramér-Rao lower bound; visibility

Introduction

Over the past decades, dark-field imaging using a grating interferometer has showed great promise in diverse fields^[1], as it is compatible with conventional sources, including X-ray tube sources^[2] and neutrons^[3], and does not require high temporal coherence^[4]. Especially, dark-field imaging can provide information about the object's microstructures on a scale below the spatial resolution of the grating interferometer, and also enables visualization of spatially-resolved small-angle scattering properties^[5-6]. In recent years, X-ray dark-field imaging with a grating interferometer has shown to provide significant benefits for several applications, including but not limited to: mammography^[7], pulmonary imaging^[8], materials analysis^[9], security screening^[10] and food sciences^[11]. Meanwhile, neutron dark-field imaging using a Talbot-Lau interferometer also has shown great potential in non-destructive testing of metallic materials^[12], research on magnetic materials^[13-14], and so

on, owing to the unique neutron features of high penetration and magnetic moment.

In grating interferometry, several methods have been developed for quantitative signal retrieval from measured intensities^[15-20]. Among them, the phase stepping (PS) technique is routinely used as the standard approach^[19,21]. The noise performance of the 3 signals retrieved with PS technique have been theoretically analyzed and experimentally validated^[22-25]. However, previous studies demonstrated that the noise variances of amplitude and phase signals obtained with a grating interferometer were always higher than Cramér-Rao lower bound (CRLB)^[26]. Numerical results implied a sub-optimality of PS technique for refraction and dark-field imaging in terms of noise variance^[27]. Their results also suggested the necessity of developing advanced retrieval algorithms to further reduce the noise variance and improve dose efficiency. Recently, reference [28] discussed the noise standard deviation and algorithm efficiency of phase shifting interferometry theoretically and numerically using CRLB. Although their studies were presented in terms of the optical pathlength, the obtained results were also applicable to grating-based refraction imaging, with some mathematical transforms. However, there still lacks of a comprehensive evaluation on the algorithm performance with respect to dark-field imaging using a grating interferometer.

Herein the performance of the PS technique for dark-field retrieval using CRLB is evaluated. Analytical

Received: 2023-03-24

Supported by the National Natural Science Foundation of China (U1532113, 11475170, 11905041), and the Fundamental Research Funds for the Central Universities (PA2020GDKC0024, JZ2022HGTB0244)

Leading author: LIU Bo, Master, Research Direction: X-ray phase contrast imaging, E-mail: 18810659522@163.com

Corresponding author: WANG Zhili, Doctor, Professor, Research Direction: X-ray phase contrast imaging, E-mail: dywangzl@hfut.edu.cn

expressions of CRLB were derived for 3-step and 4-step PS techniques, respectively. Through numerical simulations, we discussed the dependence of the CRLB and algorithm efficiency on various experimental parameters, including the mean intensity, the phase step number and the visibility. The presented results can be useful for advanced algorithm development and further noise reduction in grating-based dark-field imaging.

1 Theory and methods

1.1 Signal retrieval by PS technique

In grating interferometer, the PS technique is commonly used as the standard approach for data acquisition and retrieval of multi-contrast signals. In data acquisition, one of the gratings is translated laterally over its period with a total of N phase step, while intensity measurements are performed at each phase step. For each detector pixel, the measured intensity oscillation I_k for a phase step k can be expressed as^[2]:

$$I_k = I_0 \left[1 + V \cos \left(\phi + 2\pi \frac{k}{N} \right) \right] \quad (1 \leq k \leq N) \quad (1)$$

where I_0 , V , and ϕ denote the mean intensity, the visibility, and the phase of the intensity oscillation, respectively, and N is the total number of phase step. For notation brevity, the spatial dependence of all terms has been omitted in Eq. (1). Subsequently, we can readily retrieve the mean intensity I_0 , the phase ϕ and the visibility V by

$$I_0 = \frac{1}{N} \sum_{k=1}^N I_k \quad (2)$$

$$\phi = -\tan^{-1} \left[\frac{\sum_{k=1}^N I_k \sin \left(2\pi \frac{k}{N} \right)}{\sum_{k=1}^N I_k \cos \left(2\pi \frac{k}{N} \right)} \right] \quad (3)$$

$$V = 2 \sqrt{\frac{\left[\sum_{k=1}^N I_k \sin \left(2\pi \frac{k}{N} \right) \right]^2 + \left[\sum_{k=1}^N I_k \cos \left(2\pi \frac{k}{N} \right) \right]^2}{\sum_{k=1}^N I_k}} \quad (4)$$

In order to quantitatively retrieve the transmission, refraction, and dark-field signals, one needs to compare measurements with a sample in the beam, to reference measurements without sample, and thereby deduce the local changes of the intensity oscillation induced by the sample. In the following, the superscripts s and r will consistently denote the values measured with the sample in place and as a reference without. The transmission signal T is calculated by the negative logarithm of the ratio of the mean intensity with sample I_0^s and without I_0^r :

$$T = -\ln(I_0^s/I_0^r) = \left[\int \mu(x, y, z) dz \right] \quad (5)$$

Where $\mu(x, y, z)$ denotes the sample's linear attenuation coefficient. The refraction signal θ_r can be obtained by the difference of the sample phase ϕ^s and the reference phase ϕ^r :

$$\theta_r = \phi^s - \phi^r \quad (6)$$

The dark-field signal D is given by the local reduction of the visibility of the intensity oscillation:

$$D = V^s/V^r \quad (7)$$

Where the V^s denotes the sample's visibility and the V^r denotes the reference's visibility. These 3 signals are calculated on a pixel-by-pixel basis, and normally displayed in the form of images.

1.2 CRLB of dark-field signal

The CRLB gives the lowest possible noise variance of the estimated parameters from a set of noisy measurements. In the following, we will use CRLB as a metric to evaluate the noise variance of the dark-field signal retrieved by the PS technique. The study also considers the Poisson distributed photon-counting noise, the most dominant noise source in real experiments, which has been validated for both X-ray and neutron imaging previously^[18, 22, 29-30].

For photon-counting detectors, the measured data follows the Poisson distribution. Under this noise model, the joint probability P of acquired intensities at all phase steps is given by

$$P(I_0, V, \phi) = \prod_{k=1}^N \frac{(\bar{I}_k)^{I_k}}{I_k!} \exp(-\bar{I}_k) \quad (8)$$

where I_k denotes the measured intensity for a phase step k , and \bar{I}_k denotes the corresponding mean value.

Secondly, the log-likelihood function L should be derived. In our case, it is

$$L(I_0, V, \phi) = \ln P(I_0, V, \phi) = \sum_{k=1}^N \{ I_k \ln \bar{I}_k - \bar{I}_k - \ln[I_k!] \} \quad (9)$$

Then taking the first partial derivatives of the log-likelihood function L with respect to I_0 , V and ϕ :

$$\frac{\partial L}{\partial I_0} = \sum_{k=1}^N \frac{I_k - \bar{I}_k}{\bar{I}_k} \left[1 + V \cos \left(\phi + 2\pi \frac{k}{N} \right) \right] \quad (10)$$

$$\frac{\partial L}{\partial V} = \sum_{k=1}^N \frac{I_k - \bar{I}_k}{\bar{I}_k} I_0 \cos \left(\phi + 2\pi \frac{k}{N} \right) \quad (11)$$

$$\frac{\partial L}{\partial \phi} = \sum_{k=1}^N \frac{I_k - \bar{I}_k}{\bar{I}_k} I_0 V \sin \left(\phi + 2\pi \frac{k}{N} \right) \quad (12)$$

Thirdly, the Fisher information matrix \mathbf{J} with respect to I_0 , V and ϕ is calculated with Eq. (13).

$$\mathbf{J} = - \begin{bmatrix} E \left[\frac{\partial^2 L}{\partial I_0^2} \right] & E \left[\frac{\partial^2 L}{\partial I_0 \partial V} \right] & E \left[\frac{\partial^2 L}{\partial I_0 \partial \phi} \right] \\ E \left[\frac{\partial^2 L}{\partial V \partial I_0} \right] & E \left[\frac{\partial^2 L}{\partial V^2} \right] & E \left[\frac{\partial^2 L}{\partial V \partial \phi} \right] \\ E \left[\frac{\partial^2 L}{\partial \phi \partial I_0} \right] & E \left[\frac{\partial^2 L}{\partial \phi \partial V} \right] & E \left[\frac{\partial^2 L}{\partial \phi^2} \right] \end{bmatrix} \quad (13)$$

where $E[\bullet]$ denotes the expectation value with respect to the given statistical model. For our Poisson distribution case, by use of Eqs.(10)-(13), we can obtain the resulting Fisher information matrix:

$$\mathbf{J} = \sum_{k=1}^N \frac{1}{\bar{I}_k} \begin{bmatrix} \frac{\partial^2 \bar{I}_k}{\partial I_0^2} & \frac{\partial^2 \bar{I}_k}{\partial I_0 \partial V} & \frac{\partial^2 \bar{I}_k}{\partial I_0 \partial \phi} \\ \frac{\partial^2 \bar{I}_k}{\partial I_0 \partial V} & \frac{\partial^2 \bar{I}_k}{\partial V^2} & \frac{\partial^2 \bar{I}_k}{\partial V \partial \phi} \\ \frac{\partial^2 \bar{I}_k}{\partial I_0 \partial \phi} & \frac{\partial^2 \bar{I}_k}{\partial V \partial \phi} & \frac{\partial^2 \bar{I}_k}{\partial \phi^2} \end{bmatrix} \quad (14)$$

where

$$\frac{\partial^2 \bar{I}_k}{\partial I_0^2} = \left[1 + V \cos \left(\phi + 2\pi \frac{k}{N} \right) \right]^2 \quad (15)$$

$$\frac{\partial^2 \bar{I}_k}{\partial V^2} = I_0^2 \cos^2 \left(\phi + 2\pi \frac{k}{N} \right) \quad (16)$$

$$\frac{\partial^2 \bar{I}_k}{\partial \phi^2} = -I_0^2 V^2 \sin \left(\phi + 2\pi \frac{k}{N} \right) \quad (17)$$

$$\frac{\partial^2 \bar{I}_k}{\partial I_0 \partial V} = I_0 \left[1 + V \cos \left(\phi + 2\pi \frac{k}{N} \right) \right] \cos \left(\phi + 2\pi \frac{k}{N} \right) \quad (18)$$

$$\begin{aligned} \frac{\partial^2 \bar{I}_k}{\partial I_0 \partial \phi} = \\ -I_0 V \left[1 + V \cos \left(\phi + 2\pi \frac{k}{N} \right) \right] \sin \left(\phi + 2\pi \frac{k}{N} \right) \end{aligned} \quad (19)$$

$$\frac{\partial^2 \bar{I}_k}{\partial V \partial \phi} = -I_0^2 V \cos \left(\phi + 2\pi \frac{k}{N} \right) \sin \left(\phi + 2\pi \frac{k}{N} \right) \quad (20)$$

And then, by inverting the Fisher information matrix, the CRLB of $[I_0, V, \phi]$ can be obtained from the diagonal element. For the visibility signal V , its CRLB is given by the second diagonal element in the inverse of Fisher information matrix. Therefore, one yields the CRLB of the visibility signal:

$$\text{CRLB}_V = [\mathbf{J}^{-1}]_{22} \quad (21)$$

Finally, by use of Eqs. (7) and (21), and error propagation formula^[29], we can obtain CRLB of the retrieved dark-field signal:

$$\text{CRLB}_D = \left(\frac{D}{V^r} \right)^2 \text{CRLB}_{V^r} + \left(\frac{1}{V^r} \right)^2 \text{CRLB}_{V^s} \quad (22)$$

1.3 Algorithm efficiency

For PS technique, the noise variance of the retrieved visibility and dark-field signals have been calculated through error propagation formula in previous studies^[22-23]. A direct comparison between CRLB and the calculated noise variance can reveal the efficiency of PS technique. The algorithm efficiency is defined as the ratio of CRLB to the calculated noise variance of dark-field signal:

$$\eta = \left(\text{CRLB}_D / \sigma_D^2 \right) \times 100\% \quad (23)$$

where the noise variance σ_D^2 can be found in reference [23].

The algorithm efficiency also indicates whether there exists any potential for algorithm improvement. In the following, the algorithm performance of several common PS techniques in the dark-field retrieval will be evaluated. On the basis of general expressions derived above, the theoretical formulae of CRLB and the algorithm efficiency of common PS techniques are presented and discussed.

1.3.1 3-step PS technique The 3-step PS technique use the least number of intensity measurements to retrieve the transmission, refraction and dark-field signals quantitatively^[18-19]. Computing the Fisher information matrix and finding the inverse matrix will lead to CRLB. With trivial mathematical computations, we can obtain CRLB of the retrieved visibility by 3-step PS technique:

$$\text{CRLB}_V^3 = \frac{2 - V^2 + V \cos(3\phi)}{3I_0} \quad (24)$$

By use of Eqs. (22) and (24), we can yield the corresponding CRLB of the retrieved dark-field signal using 3-step PS technique:

$$\begin{aligned} \text{CRLB}_D^3 = \\ \frac{D^2}{3} \left\{ \frac{1}{I_0^r} \left[\frac{2}{(V^r)^2} - 1 + \frac{\cos(3\phi^r)}{V^r} \right] + \frac{1}{I_0^s} \left[\frac{2}{(V^s)^2} - 1 + \frac{\cos(3\phi^s)}{V^s} \right] \right\} \end{aligned} \quad (25)$$

Previous studies has reported the noise variance of 3-step PS technique for retrieved dark-field signals^[23], and the expression is actually identical to Eq. (25), which means that if extrinsic noise can be eliminated, the 3-step PS technique can reach the theoretically optimal noise efficiency. In other words, this algorithm is fully efficient (i.e., $\eta = 100\%$) according to Eq.(23). A similar result has been observed for CRLB of the retrieved refraction signal^[28, 31]. It is worth noting that fully efficient

algorithms are currently available only for 3-step PS technique, and other PS techniques with more phase steps are all sub-optimal, as discussed in the following.

1.3.2 4-step PS technique Similar to the case of 3-step PS technique, by calculating the diagonal elements of the inverse of the Fisher information matrix, we can obtain CRLB of the retrieved visibility by 4-step PS technique:

$$\text{CRLB}_V^4 = \frac{4 - 3V^2 - V^2 \cos 4\phi}{8I_0} \quad (26)$$

By use of Eqs. (22) and (26), we can yield the CRLB of the retrieved dark-field signal:

$$\text{CRLB}_V^4 = \frac{D^2}{4} \left\{ \frac{1}{I_0^r} \left[\frac{2}{(V^r)^2} - 1 - \frac{1 + \cos(4\phi^r)}{2} \right] + \frac{1}{I_0^s} \left[\frac{2}{(V^s)^2} - 1 - \frac{1 + \cos(4\phi^s)}{2} \right] \right\} \quad (27)$$

Previous studies reported the noise variance of the retrieved dark-field signal by 4-step PS technique as^[23]:

$$\sigma_D^2 = \frac{D^2}{4} \left\{ \frac{1}{I_0^r} \left[\frac{2}{(V^r)^2} - 1 \right] + \frac{1}{I_0^s} \left[\frac{2}{(V^s)^2} - 1 \right] \right\} \quad (28)$$

Different from the CRLB in Eq. (27), the noise variance is independent of the phases ϕ^s and ϕ^r . By use of Eqs. (27) and (28), we can calculate the algorithm efficiency of 4-step PS technique as:

$$\eta_4 = \frac{\left[\frac{2}{(V^r)^2} - 1 - \frac{1 + \cos(4\phi^r)}{2} \right] + \frac{I_0^r}{I_0^s} \left[\frac{2}{(V^s)^2} - 1 - \frac{1 + \cos(4\phi^s)}{2} \right]}{\left[\frac{2}{(V^r)^2} - 1 \right] + \frac{I_0^r}{I_0^s} \left[\frac{2}{(V^s)^2} - 1 \right]} \times 100\% \quad (29)$$

As revealed by Eq.(29), the algorithm efficiency η_4 is generally lower than 100%, which indicates that 4-step PS technique is sub-optimal in terms of the noise of the retrieved dark-field signal. Only at specific isolated locations determined by $\phi^r = (2m + 1)\pi/4$ and $\phi^s = (2n + 1)\pi/4$, with m, n both being integers, the algorithm efficiency reaches 100%, meaning that the noise variance is equal to the CRLB at these locations.

1.3.3 N -step PS technique ($N \geq 5$) In order to effectively remove the effect of higher orders in obtaining Eq.(1), a larger integer is selected for N ^[21]. Since analytical expression of CRLB of the dark-field signal retrieved by N -step PS technique is difficult to be simplified, we will compute these bounds numerically in the following.

The noise variance of the dark-field signal retrieved by N -step PS technique was^[23]:

$$\sigma_D^2 = \frac{D^2}{N} \left\{ \frac{1}{I_0^r} \left[\frac{2}{(V^r)^2} - 1 \right] + \frac{1}{I_0^s} \left[\frac{2}{(V^s)^2} - 1 \right] \right\} \quad (30)$$

For further analysis, the algorithm performance of N -step PS technique will be evaluated by calculating the CRLB numerically and comparing it with the corresponding noise variance in Eq.(30). Especially, the dependences of the algorithm efficiency on the mean intensity, the phase step number and the visibility are investigated systematically.

2 Results and discussions

The developed models of CRLB are validated by numerical calculations, and some quantitative insights into the algorithm efficiency is further provided. In order to obtain results independent of the sample, we further restricted the analysis to a sample-free region within the retrieved dark-field image^[32]. Note that this choice is commonly made in experimental measurements^[18, 23]. Therefore, the mean intensity, the visibility, and the phase are equal for the reference and sample measurements, and the noise is determined by calculating the variance over a background region of 80×80 pixels.

As revealed by Eqs. (24) and (27), the CRLB of retrieved dark-field signals exhibits a periodic oscillation as a function of the phases ϕ^s and ϕ^r . Similar results were obtained for CRLB of refraction signals^[28]. By contrast, the calculated noise variance is independent of the phase distribution, with a phase step number greater than 3. Therefore, we investigated the dependence of CRLB of dark-field signals on the phase distribution. For this purpose, we calculated the ratio of the oscillation amplitude to the corresponding average as a function of the phase step number for different representative visibilities (Figure 1). As expected, the ratio decreases monotonically when the phase step number increases, indicating a larger phase step number is effective to remove the effect of phase distribution. With a high visibility of 0.74, the ratios are 23% and 10% for 4-step and 5-step PS techniques, respectively, which means that the substantial effect of the phase distribution on CRLB can not be neglected. With a phase step number greater than 5, the ratio decreases to less than 5%. The phase distribution is considered to have a negligible contribution

to CRLB. Then we can reasonably take the average value of CRLB to evaluate the algorithm efficiency. With a lower visibility (0.30 and 0.50), the ratio is always below 10%, meaning that the phase distribution has an insignificant effect on CRLB. Based on results shown in Figure 1, for an impartial and convenient comparison, the average value of CRLB will be used for algorithm efficiency evaluations in the following.

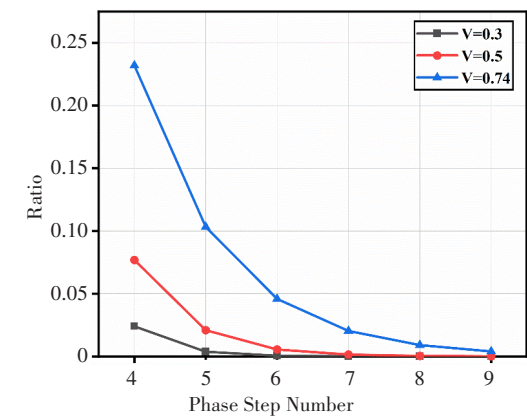


Figure 1 Ratio of oscillation amplitude to its average against the phase step number for different visibilities (V)

The dependency of CRLB of dark-field signals on the mean intensity is investigated to test the validity of these theoretical models. The calculated results are shown in Figure 2, where the logarithm of CRLB is plotted against the logarithm of the mean intensity, together with the least-squares fitting, for different phase steps and visibilities. The fitted slopes are summarized in Table 1. As expected, the CRLB of dark-field signals decreases monotonically with the mean intensity. From the least-squares fitting results, we can conclude that CRLB of retrieved dark-field signals is inversely proportional to the mean intensity, which is consistent with Eqs. (25) and (27). In addition, a similar behavior has been observed for the noise variance^[23]. Based on these results, we can expect the algorithm efficiency is independent of the mean intensity.

Moreover, we investigated the dependency of CRLB and the noise variance on the phase step number in the case of different visibilities. As shown in Figure 3a, the logarithm of CRLB and noise variance are plotted against the logarithm of the phase step number, where the noise

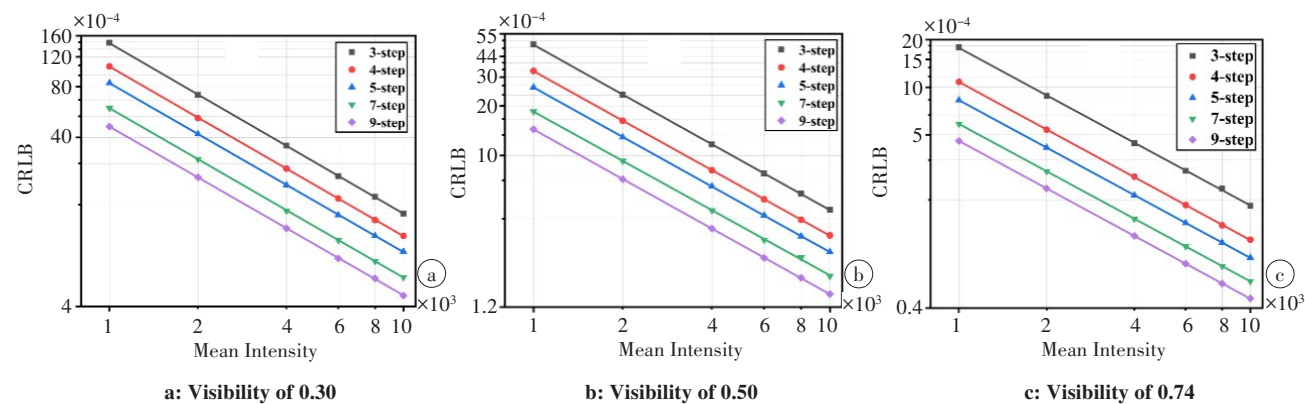


Figure 2 Log-log plot of CRLB of retrieved dark-field signals as a function of the mean intensity, together with the least-squares fitting

Table 1 Fitted slopes of Figure 2

Number of phase step	Visibility		
	0.30	0.50	0.74
3	1.009±0.003	1.005±0.002	0.997±0.002
4	1.004±0.002	1.003±0.003	1.002±0.001
5	0.998±0.002	1.002±0.001	0.997±0.002
7	1.003±0.002	0.995±0.002	0.997±0.001
9	0.998±0.001	1.002±0.001	0.998±0.001

variance is abbreviated as Var, and the mean intensity is assumed to 2 000 for those calculations. As expected, both

CRLB and noise variance exhibit a monotonic decrease with increasing phase step number for different visibilities. While the noise variance is inversely proportional to the phase step number, the CRLB decreases nonlinearly with the phase step number. Besides, the CRLB is always no greater than the noise variance in all presented representative experimental cases; and the difference between CRLB and the noise variance varies with the phase step number and the visibility. As seen from Figure 3a, with a low visibility of 0.30, a typical value in laboratory experiments^[15], the

difference is insignificant, regardless of the phase step number. With the visibility increased to 0.50, representative of synchrotron experimental visibilities^[18], the difference becomes more obvious with an increase in the phase step number. With a high visibility of 0.74, the highest visibilities reported in experimental studies^[33], the difference between CRLB and noise variance becomes quite significant. These results suggest a strong dependence of the algorithm efficiency on the visibility.

Furthermore, to quantitatively evaluate the difference between CRLB and the noise variance, the algorithm efficiency is calculated and the results are displayed in Figure 3b. With a low visibility of 0.30, the algorithm efficiency shows a slight decrease with an increased phase step number, and remains greater than 97%, even with a large phase step number, which means that with a low visibility, the PS technique has an excellent performance for dark-field retrieval. With an increased visibility of

0.50, the algorithm efficiency decreases from 100% to 92.9% when the phase step number increases from 3 to 4. With a phase step number of 5, the algorithm efficiency slightly decreases to 92.4%. When the phase step number increases further, the algorithm efficiency remains almost the same value. Therefore, it can be concluded that the algorithm efficiency is greater than 92% with a visibility of 0.5, indicating some room for potential improvement. With a high visibility of 0.74, we observe a dramatic decrease in the algorithm efficiency when the phase step number increases from 3 to 4. Quantitatively, the algorithm efficiency decreases from 100% to 81.1%. With a phase step number of 5, the algorithm efficiency further drops to 77.5%; and with further increase in the phase step number, the algorithm efficiency does not decrease significantly and becomes nearly constant. The algorithm efficiency even lower than 80%, indicating that the PS technique has a great potential for improvement.

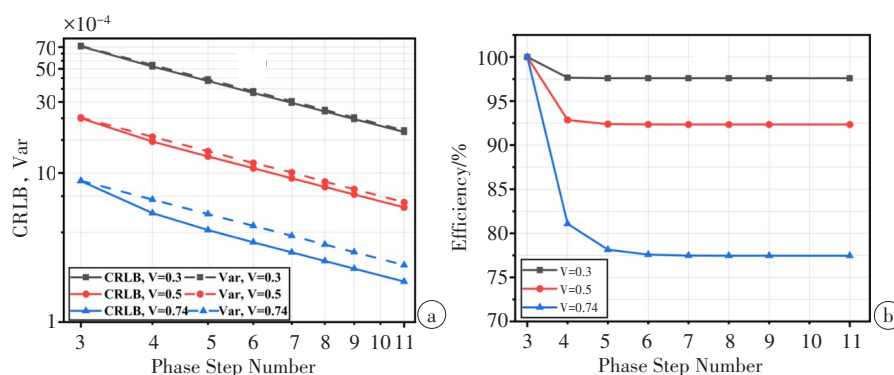


Figure 3 (a) Log-log plot of CRLB and the noise variance of retrieved dark-field signals as a function of the phase step number in the case of different visibilities; and (b) algorithm efficiency as a function of the phase step number for different visibilities

Besides, the dependence of CRLB and the noise variance on the visibility in the case of different phase steps is also investigated. Figure 4a shows the logarithm of calculated CRLB and noise variance as a function of the visibility, where the mean intensity is assumed to be 2 000. Both CRLB and noise variance of retrieved dark-field signals decrease monotonically as the visibility increases. For 3-step PS technique, noise variance always coincides with CRLB, regardless of the visibility. With a phase step number greater than 3, the difference gap between noise variance and CRLB increases substantially with an increase in the visibility.

For a quantitative evaluation, Figure 4b displays the

algorithm efficiency with respect to the visibility for different phase steps. As demonstrated, the algorithm efficiency of 3-step PS technique always has a value of 100%, and does not change with the visibility. This result is in agreement with previous theoretical predictions. When the visibility increases from 0.20 to 0.74, the algorithm efficiency of 4-step PS technique decreases from 98.9% to 81.1%, and that of 5-step PS technique decreases from 98.9% to 78.1%, and that for a phase step greater than 5 decreases from 98.9% to 77.4%. More importantly, the overlapping of the algorithm efficiency curves indicates that further increasing the phase step number will not improve the algorithm efficiency.

The results shown in Figures 3 and 4 clearly demonstrate that for dark-field retrieval, the efficiency of the PS technique decreases significantly with a large phase step number and a high visibility. Especially noting the ongoing

increase in the visibility^[33-35], those results emphasize the necessity of advanced algorithm development for dark-field retrieval with a reduced noise variance.

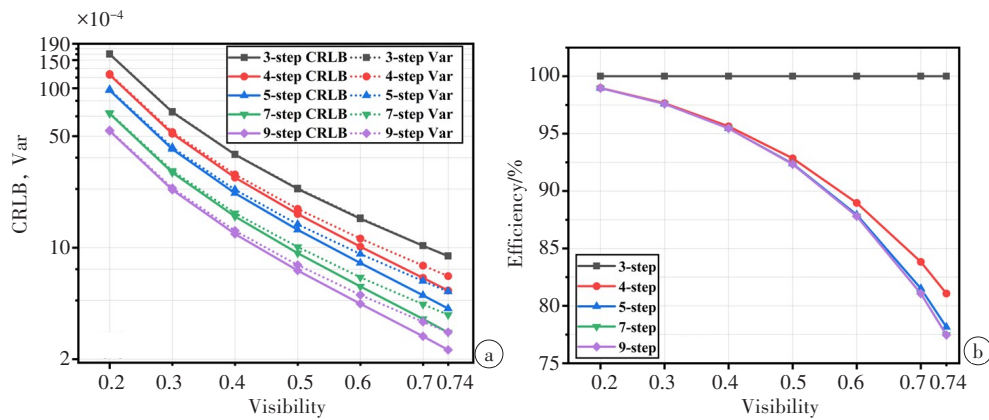


Figure 4 (a) Logarithm of CRLB and the noise variance of retrieved dark-field signals as a function of the visibility for different phase step number; and (b) algorithm efficiency as a function of the visibility for different phase step number

Finally, as a complement to previous studies^[28], we evaluate the algorithm efficiency of the PS technique for refraction retrieval. The dependence of the algorithm efficiency on the phase step number and the visibility is illustrated in Figure 5. A similar behavior is observed between the algorithm efficiency of refraction retrieval and dark-field retrieval. It is shown that the algorithm efficiency of the 3-step PS technique is always 100%, and does not change with the visibility, which is consistent with dark-field retrieval. Compared with the dark-field retrieval, the algorithm efficiency for refraction retrieval is always higher for the same phase step number and visibility, with a phase step greater than 3. Meanwhile, it

is also worthy to note that with a high visibility of 0.74, the algorithm efficiency is 83.6% when the phase step number is greater than 5, which again suggests the substantial potential for noise variance reduction.

The results shown in Figures 3, 4 and 5 demonstrate that with a low visibility, the PS technique is indeed an efficient technique for refraction retrieval and dark-field retrieval. However, with a high visibility and a large phase step number, the efficiency of the PS technique decreases significantly, especially for the dark-field retrieval. Therefore, it becomes necessary to develop advanced techniques for refraction retrieval and dark-field retrieval with a reduced noise variance.

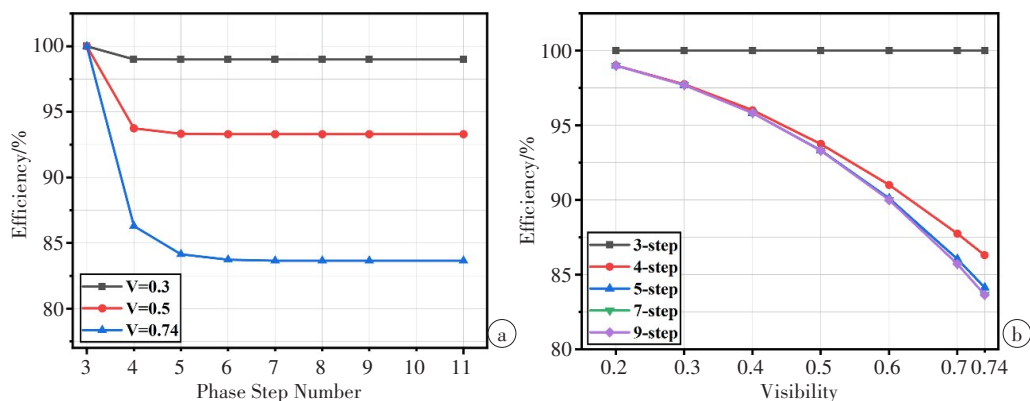


Figure 5 (a) Algorithm efficiency of refraction retrieval as a function of the phase step number for different visibilities; and (b) algorithm efficiency of refraction retrieval as a function of the visibility for different phase step number

3 Conclusion

The study evaluated the algorithm performance of the PS technique for dark-field retrieval using CRLB. Specifically, analytical expressions of CRLB are theoretically derived for 3-step and 4-step PS techniques, respectively. Through theoretical analysis and numerical calculations, it is shown that fully efficient algorithm is currently available only for 3-step PS technique and other techniques with more steps are all sub-optimal. Furthermore, we investigated the dependence of the algorithm efficiency on the phase step number and the visibility, respectively. The results demonstrate that the PS technique can nearly approach its theoretical optimal efficiency in the case of a low visibility of 0.30. With an increase in the visibility, the efficiency decreases significantly, with a phase step greater than 3. Since the mean intensity is directly linked to the radiation dose, a lower noise variance of retrieved dark-field and refraction signals retrieval means superior dose efficiency. It is expected that the presented results can be used for further noise reduction and potential dose optimizations of grating-based dark-field and refraction imaging.

References

- [1] Kardjilov N, Manke I, Woracek R, et al. Advances in neutron imaging [J]. Mater Today, 2018, 21(6): 652-672.
- [2] Pfeiffer F, Bech M, Bunk O, et al. Hard-X-ray dark-field imaging using a grating interferometer[J]. Nat Mater, 2008, 7(2): 134-137.
- [3] Strobl M, Grunzweig C, Hilger A, et al. Neutron dark-field tomography [J]. Phys Rev Lett, 2008, 101(12): 123902.
- [4] Bravin A, Coan P, Suortti P. X-ray phase-contrast imaging: from pre-clinical applications towards clinics[J]. Phys Med Biol, 2013, 58(1): R1-R35.
- [5] Yashiro W, Terui Y, Kawabata K, et al. On the origin of visibility contrast in X-ray Talbot interferometry[J]. Opt Express, 2010, 18(16): 16890-16901.
- [6] Strobl M. General solution for quantitative dark-field contrast imaging with grating interferometers[J]. Sci Rep, 2014, 4: 7243.
- [7] Rauch T, Rieger J, Pelzer G, et al. Discrimination analysis of breast calcifications using X-ray dark-field radiography[J]. Med Phys, 2020, 47(4): 1813-1826.
- [8] Willer K, Fingerle AA, Noichl W, et al. X-ray dark-field chest imaging for detection and quantification of emphysema in patients with chronic obstructive pulmonary disease: a diagnostic accuracy study[J]. Lancet Digital Health, 2021, 3(11): e733-e744.
- [9] Kim J, Kagias M, Marone F, et al. X-ray scattering tensor tomography with circular gratings[J]. Appl Phys Lett, 2020, 116(13): 134102.
- [10] Miller EA, White TA, McDonald BS, et al. Phase contrast X-Ray imaging signatures for security applications[J]. IEEE Trans Nucl Sci, 2013, 60(1): 416-422.
- [11] Nielsen MS, Damkjær KB, Feidenhansl R. Quantitative *in-situ* monitoring of germinating barley seeds using X-ray dark-field radiography[J]. J Food Eng, 2017, 198: 98-104.
- [12] Brooks AJ, Hussey DS, Yao H, et al. Neutron interferometry detection of early crack formation caused by bending fatigue in additively manufactured SS316 dogbones[J]. Mater Design, 2018, 140: 420-430.
- [13] Betz B, Rauscher P, Harti RP, et al. Magnetization response of the bulk and supplementary magnetic domain structure in high-permeability steel laminations visualized *in situ* by neutron dark-field imaging[J]. Phys Rev Lett, 2016, 6(2): 024023.
- [14] Harti RP, Strobl M, Schafer R, et al. Dynamic volume magnetic domain wall imaging in grain oriented electrical steel at power frequencies with accumulative high-frame rate neutron dark-field imaging[J]. Sci Rep, 2018, 8(1): 15754.
- [15] Marschner M, Birnbacher L, Mechlem K, et al. Two-shot X-ray dark-field imaging[J]. Opt Express, 2016, 24(23): 27032-27045.
- [16] Li PY, Zhang K, Bao Y, et al. Angular signal radiography[J]. Opt Express, 2016, 24(6): 5829-5845.
- [17] Bevins N, Zambelli J, Li K, et al. Multicontrast X-ray computed tomography imaging using Talbot-Lau interferometry without phase stepping[J]. Med Phys, 2012, 39(1): 424-428.
- [18] Wang ZL, Shi XM, Ren K, et al. Transmission, refraction and dark-field retrieval in hard X-ray grating interferometry[J]. J Synchrotron Radiat, 2020, 27(2): 494-502.
- [19] Weitkamp T, Diaz A, David C, et al. X-ray phase imaging with a grating interferometer[J]. Opt Express, 2005, 13(16): 6296-6304.
- [20] Wang ZL, Ren K, Shi XM, et al. Technical Note: single-shot phase retrieval method for synchrotron-based high-energy X-ray grating interferometry[J]. Med Phys, 2019, 46(3): 1317-1322.
- [21] Momose A, Yashiro W, Takeda Y, et al. Phase tomography by X-ray talbot interferometry for biological imaging[J]. JPN J Appl Phys, 2006, 45(6A): 5254-5262.
- [22] Revol V, Kottler C, Kaufmann R, et al. Noise analysis of grating-based X-ray differential phase contrast imaging[J]. Rev Sci Instrum, 2010, 81(7): 073709.
- [23] Wang ZL, Xu W, Wang TX, et al. Revised noise model of dark-field imaging using a grating interferometer[J]. Nucl Instrum Meth A, 2021, 995: 165113.
- [24] Weber T, Bartl P, Bayer F, et al. Noise in X-ray grating-based phase-contrast imaging[J]. Med Phys, 2011, 38(7): 4133-4140.
- [25] 杨萌, 胡仁芳, 王圣浩, 等. X射线光栅相位衬度成像技术中背景扣除方法的比较[J]. 中国医学物理学杂志, 2017, 34(7): 649-659.
- [25] Yang M, Hu RF, Wang SH, et al. Background correction methods in X-ray phase-contrast imaging with Talbot-Lau interferometer: a comparative study[J]. Chinese Journal of Medical Physics, 2017, 34(7): 649-659.
- [26] Kay SM. Fundamentals of statistical signal processing[M]. 2nd ed. Englewood Cliffs: Prentice-Hall, Inc., 1993.
- [27] Ge YS, Li K, Chen GH. Cramér-Rao lower bound in differential phase contrast imaging and its application in the optimization of data acquisition systems[C]. Proceedings of SPIE, 2014. DOI: 10.1117/12.2043930.
- [28] Chen S, Zhu Y. Phase sensitivity evaluation and its application to phase shifting interferometry[J]. Methods, 2018, 136: 50-59.
- [29] Harti RP, Strobl M, Morgano M, et al. Statistical uncertainty in the dark-field and transmission signal of grating interferometry[J]. Rev Sci Instrum, 2017, 88(10): 103704.
- [30] Chabior M, Donath T, David C, et al. Signal-to-noise ratio in X ray dark-field imaging using a grating interferometer[J]. J Appl Phys, 2011, 110(5): 053105.
- [31] Wu Z, Gao K, Chen J, et al. High sensitivity phase retrieval method in grating-based X-ray phase contrast imaging[J]. Med Phys, 2015, 42(2): 741-749.
- [32] Massimi L, Partridge T, Astolfo A, et al. Optimization of multipoint phase retrieval in edge illumination X-ray imaging: a theoretical and experimental analysis[J]. Med Phys, 2021, 48(10): 5884-5896.
- [33] Neuwirth T, Backs A, Gustschin A, et al. A high visibility Talbot-Lau neutron grating interferometer to investigate stress-induced magnetic degradation in electrical steel[J]. Sci Rep, 2020, 10(1): 1764.
- [34] Rieger J, Meyer P, Pelzer G, et al. Designing the phase grating for Talbot-Lau phase-contrast imaging systems: a simulation and experiment study[J]. Opt Express, 2016, 24(12): 13357-13364.
- [35] Weber T, Pelzer G, Rieger J, et al. Report of improved performance in Talbot-Lau phase-contrast computed tomography[J]. Med Phys, 2015, 42(6): 2892-2896.

(编辑:谭斯允)

基于光栅干涉仪的暗场成像的Cramér-Rao下界

刘波,陈子涵,顾瑶,陈恒,王志立

合肥工业大学物理学院光学工程系,安徽 合肥 230009

【摘要】在光栅相衬成像中,通常使用相位步进法进行数据采集和信息提取。然而,对于相位步进法在提取暗场信号的算法效率还没有得到充分的评估。本研究引入Cramér-Rao下界对提取暗场信号的算法效率进行评估。基于理论分析和数值计算发现目前完全有效的算法仅适用于三步相位步进法,其他更多步数的相位步进法都是次优的。本研究以Cramér-Rao下界作为依据,定量地分析了相位步进数和可见度对算法效率的影响。结果表明在低可见度的情况下,相位步进法可以接近理论的最佳效率;在高可见度的情况下,当相位步进数大于5时,算法效率仅为77.4%,这可为基于X射线和中子光栅干涉仪的暗场成像的信噪比优化提高、剂量优化提供指导。

【关键词】暗场成像;光栅干涉仪;Cramér-Rao下界;可见度

【中图分类号】R318;R811.1

【文献标志码】A

【文章编号】1005-202X(2023)09-1105-09

【收稿日期】2023-03-24

【基金项目】国家自然科学基金(U1532113, 11475170, 11905041);中央高校基本科研基金(PA2020GDKC0024, JZ2022HGTB0244)

【作者简介】刘波,硕士,研究方向:X射线相衬成像,E-mail: 18810659522@163.com

【通信作者】王志立,博士,教授,研究方向:X射线相衬成像,E-mail: dywangzl@hfut.edu.cn